The intercept of the line with the abscissa yields ΔV. This geometry-independent constant is characteristic for the specific nanotube under investigation and is typically on the order of several volts. Similarly, attaching nanoscopic conducting particles to the nanotubes facilitates measurements of their work functions.

The methods developed here are also well suited to measure masses in the picogram-to-femtogram mass range, as demonstrated in Fig. 4A, which shows the resonance of a carbon particle that is attached to the end of a nanotube (*38*). The mass of this particle was determined from the resonance frequency of the structure and was found to be $M = 22 \pm 6$ fg (1 fg = 10^{-15} g). This value is near that calculated from the measured geometry, assuming bulk amorphous carbon density—that is, $M \approx 30$ fg. This nanobalance method can be applied to other particles of similar dimensions, such as viruses.

References and Notes

1. S. Iijima, *Nature* **354**, 56 (1991).
2. J. W. Mintmire, B. I. Dunlap, C. T. White, *Phys. Rev. Lett.* **68**, 631 (1992).
3. M. S. Dresselhaus, G. Dresselhaus, R. Saito, *Carbon* **33**, 883 (1995).
4. D. L. Carroll *et al.*, *Phys. Rev. Lett.* **78**, 2811 (1997).
5. T. W. Ebbesen, *Phys. Today* **49**, 26 (1996).
6. W. A. de Heer, A. Chatelain, D. Ugarte, *Science* **270**, 1179 (1995).
7. S. Frank, P. Poncharal, Z. L. Wang, W. A. de Heer, *ibid.* **280**, 1744 (1998).
8. J. Liu *et al.*, *ibid.*, p. 1253.
9. A. Thess *et al.*, *ibid.* **273**, 483 (1996).
10. D. H. Robertson, D. W. Brenner, J. W. Mintmire, *Phys. Rev. B* **45**, 12592 (1992).
11. R. S. Ruoff and D. C. Lorents, *Carbon* **33**, 925 (1995).
12. M. M. Treacy, T. W. Ebbesen, J. M. Gibson, *Nature* **38**, 678 (1996).
13. B. I. Yakobson, C. J. Brabec, J. Bernholc, *Phys. Rev. Lett.* **76**, 2511 (1996).
14. M. R. Falvo *et al.*, *Nature* **389**, 582 (1997).
15. J. P. Lu, *Phys. Rev. Lett.* **79**, 1297 (1997).
16. E. Wong, P. Sheehan, C. Lieber, *Science* **277**, 1971 (1997).
17. C.-H. Kiang *et al.*, *Phys. Rev. Lett.* **81**, 1869 (1998).
18. W. H. Knechte *et al.*, *Appl. Phys. Lett.* **73**, 1961 (1998).
19. S. Iijima, C. Brabeck, A. Maiti, J. Bernholc, *J. Chem. Phys.* **104**, 2089 (1996).
20. T. Kuzumaki *et al.*, *Phil. Mag. A* **77**, 1461 (1998).
21. J.-P. Salvetat *et al.*, *Adv. Mat.*, in press.
22. N. Yao and V. Lordi, *J. Appl. Phys.* **84**, 1939 (1998).
23. G. Gao, T. Cagin, W. A. Goddard, *Nanotechnology* **9**, 184 (1998).
24. B. T. Kelly, *Physics of Graphite* (Applied Science, London, 1981).
25. N. Osakabe *et al.*, *Appl. Phys. Lett.* **70**, 940 (1997).
26. T. W. Ebbesen and P. M. Ajayan, *Nature* **358**, 220 (1992). We caution that different production recipes can yield different results; in particular, defect densities may vary substantially from one laboratory to the next (as is the case with crystal growing). For example, catalytically grown tubes are usually very defective. In contrast, the nanotube material used in this work [including (*31*)] was from the same stock as was used in our previous work (*6*, *7*) and was of high quality.
27. The TEM used was a JEOL 100C (100 kV) at the School of Materials Science and Engineering, Georgia Institute of Technology.
28. D. J. Griffiths and Y. Li, *Am. J. Phys.* **64**, 706 (1996).
29. L. Meirovich, *Elements of Vibration Analysis* (McGraw-Hill, New York, ed. 2, 1986).
30. D_i was not measured for all nanotubes, and in those cases it was not included in the calculations. However, the value for E is rather insensitive to D_i, because $D_i/D = 1/4$, which is an extreme case, differs only by 7% as compared with $D_i = 0$.
31. Microscopy was performed with a Philips CM30 200-kV high-resolution TEM.
32. The ripple mode may be a precursor to buckling, but it should not be confused with bucking. Buckling (in contrast to rippling) is characterized as an instability giving rise to a nonlinear response. It occurs in highly stressed nanotubes (and beams) and manifests as one or several kinks with very small radii of curvature (about 1 to 10 nm). It is accompanied by abrupt change in the effective force constant and may cause irreversible damage. The observed effect may be related to the rippling found in classical beams as a precursor to buckling [see S. Kyriakides and G. T. Ju, *Int. J. Solids Struct.* **29**, 1117 (1992)].
33. In the bulk, the other elastic moduli are at least a factor of 5 and as much as a factor of 50 smaller than that of C_{11}.
34. D. Ugarte, *Nature* **352**, 707 (1992).
35. Lord Kelvin, *Philos. Mag.* **46**, 82 (1898).
36. N. A. Sulpice and R. J. D'Arcy, *J. Phys. E* **3**, 477 (1970).
37. Electrical charging due to the electron beam cannot account for the effect, because the charge found to reside on the nanotubes is positive rather than negative. Furthermore, the amplitude of vibration at resonance does not change with electron dose, as it would if electron beam charging were important.
38. M. Gurgoze, *J. Sound Vib.* **190**, 149 (1996).

39. We thank U. Landman, R. L. Whetten, L. Forro, and A. Zangwill for fruitful discussion and R. Nitsche for his analysis of the static bent nanotube. D.U. thanks the Centre Interdepartemental de Microscopy Electronique, Ecole Polytechnique Federale, for the use of the Philips CM30 microscope for Fig. 3, B through D, and the Brazilian Council for Scientific and Technological Research. Supported by the Army Research Office, grants DAAG 55-97-0133 (W.A.d.H. and P.P.), by NSF9733160 (Z.L.W.), and by NSFDMR-9971412 (W.A.d.H. and Z.L.W.)

4 December 1998; accepted 26 January 1999

An Elusive Blind-Thrust Fault Beneath Metropolitan Los Angeles

John H. Shaw[1]* and Peter M. Shearer[2]

Seismic reflection profiles, petroleum wells, and relocated earthquakes reveal the presence of an active blind-thrust fault beneath metropolitan Los Angeles. A segment of this fault likely caused the 1987 Whittier Narrows (magnitude 6.0) earthquake. Mapped sizes of other fault segments suggest that the system is capable of much larger (magnitude 6.5 to 7) and more destructive earthquakes.

Damages exceeding $35 billion from the 1994 Northridge [magnitude (M) 6.7] earthquake (*1*), combined with recent evidence of larger ($>M$ 7) events in the geologic record (*2*), have focused attention on the hazards posed by thrust faults to metropolitan Los Angeles. Efforts to assess and mitigate these hazards are complicated, however, because thrust faults beneath the city are typically blind, meaning that they lie concealed beneath Earth's surface (*3*, *4*). Here, we used high-resolution, subsurface images acquired by the petroleum industry (Fig. 1) and relocated seismicity to map a large blind-thrust system lying directly beneath the metropolitan area (Fig. 2).

Many blind thrusts produce near-surface folds that grow during repeated earthquakes (*3*–*5*) in response to motions through bends in fault planes or above propagating fault tips, and their shapes reflect underlying fault geometries and slip (*6*, *7*). Seismic reflection profiles and information from oil wells reveal a series of these anticlines extending from downtown Los Angeles to the Coyote Hills (*8*–*10*) in northern Orange County (Fig. 2). These folds grew in the Quaternary while sediments were deposited above them, yielding patterns of deformed strata that record fold growth and fault slip (*11*). These deformed strata are particularly well imaged in the Santa Fe Springs anticline (Fig. 1).

On the basis of fault-related folding theories (*11*), the shape of the growth fold at Santa Fe Springs suggests that an underlying fault, which we call the Puente Hills thrust, dips to the north and extends upward into the Pliocene Fernando Formation. This fault shape and position are consistent with a north-dipping reflection beneath the anticline that cuts across bedding. This reflection is observed on more than 10 seismic profiles and persists through a range of processing steps aimed to remove noise and artifacts (*12*). Thus, we interpret this reflection as an image of the fault surface, caused by velocity and density contrasts that exist across the fault plane.

Fault-plane reflections in a series of seismic profiles define an east-west–striking surface that dips about 27° to the north. We extrapolated beyond the limits of the fault-plane reflections, using fold shape, as imaged in the seismic profiles, to predict the fault shape (*6*, *11*) and map the fault surface (Fig. 2). The mapped fault extends 40 km along strike and includes three distinct geometric

[1]Department of Earth and Planetary Sciences, Harvard University, Cambridge, MA 02138, USA. [2]Institute of Geophysics and Planetary Physics, Scripps Institute of Oceanography, University of California, San Diego, La Jolla, CA 92093–0225, USA.

*To whom correspondence should be addressed. E-mail: shaw@eps.harvard.edu

segments, termed Los Angeles, Santa Fe Springs, and Coyote Hills. This fault system is distinct from the previously documented Elysian Park fault (*10*, *13*) and thus represents a hazard that has not been previously considered.

The mapped fault surface at Santa Fe Springs has the same strike and dip as the fault that ruptured in the 1987 Whittier Narrows (*M* 6.0) earthquake (Fig. 2). The ~25° northward dip of the Whittier Narrows mainshock, as determined by the focal mechanism (*14*) and aftershock locations (*14*, *15*), agrees with the orientation of the Puente Hills reflector. However, the projected reflector plane crosses the location of the Whittier Narrows event at a depth of about 12.8 km, 3 km deeper than the Southern California Seismograph Network (SCSN) catalog earthquake location and 2 to 3 km shallower than revised estimates of the mainshock depth from previous studies (*14*, *15*). In turn, the Whittier Narrows rupture surface from these studies projects up to relatively undeformed regions of the Puente Hills and central Los Angeles basin (*4*). Thus, we relocated the earthquakes more accurately to substantiate or eliminate this discrepancy.

We applied the L1-norm, waveform cross-correlation approach (*15*) to obtain accurate locations of the Whittier Narrows earthquake and its aftershocks. To improve the accuracy of the absolute event locations, particularly in depth, we accounted for three-dimensional velocity variations in two different ways: (i) We relocated the events using station terms (timing corrections) for SCSN stations derived from a spatially distributed set of 4800 events across southern California (*16*). These terms correct for differences in the shallow velocity structure beneath the stations. (ii) For four stations close to the Whittier Narrows earthquake (FLA, GVR, SC1, and TCC), we obtained detailed velocity information from boreholes (Fig. 3), the same data used to define the fault position in the reflection image. We relocated the events using the custom profiles at these stations and a reference one-dimensional model at all other stations. We forced an exact fit to the travel times for station FLA, the nearby station with the most data.

Both methods indicate that the Whittier Narrows events are shallower than the locations obtained without these corrections (*15*), which were biased downward by slow near-surface velocities at seismic stations close to the sequence. The station term locations place the mainshock at 12.7 km; the borehole velocity–constrained locations place the mainshock at 13.5 km. In both cases, the mainshock locates near the center of the aftershock plane, which dips ~25° to the north (Fig. 4). Formal statistical error bounds on these depth estimates are quite small (0.1 to 0.3 km), but these numbers do not include the uncertainties in the velocity model. On the basis of the depths obtained from the two methods, we estimate that the mainshock depth is 13 ± 1 km. This earth-

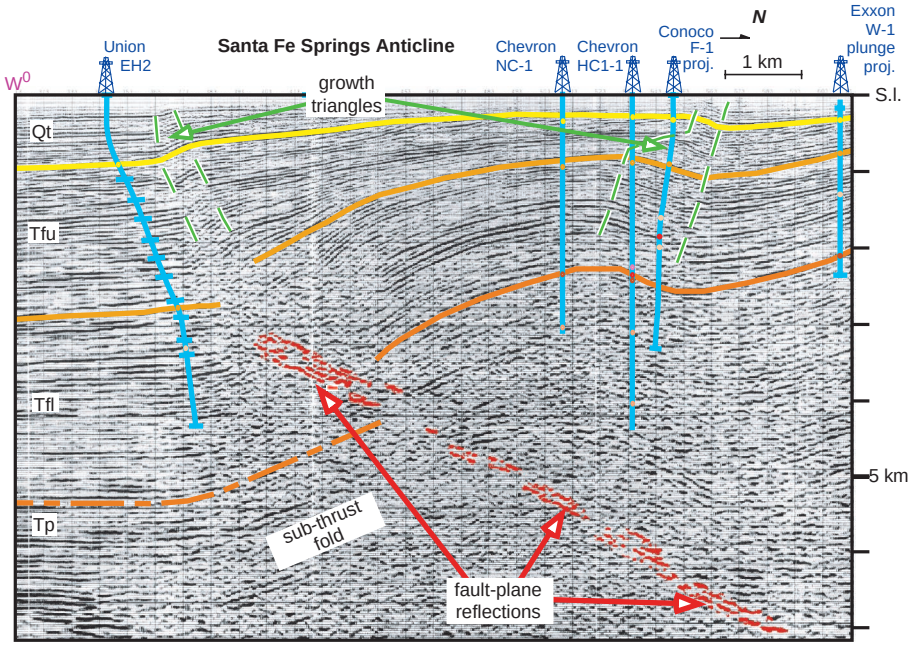

Fig. 1. Migrated seismic reflection profile imaging a segment of the Puente Hills blind-thrust system beneath the Santa Fe Springs anticline. Interpreted fault-plane reflections, selected by lateral coherence (*12*), are highlighted in red. The subthrust fold is part of the Santa Monica Mountains anticlinorium, which is developed above the Elysian Park thrust system (*4*, *5*). Qt, Quaternary; Tfu, Pliocene upper Fernando Formation; Tfl, Pliocene lower Fernando Formation; Tp, Miocene Puente Formation. Data courtesy of Texaco. An unmarked version of this figure is available at www.sciencemag.org/feature/data/984081.shl.

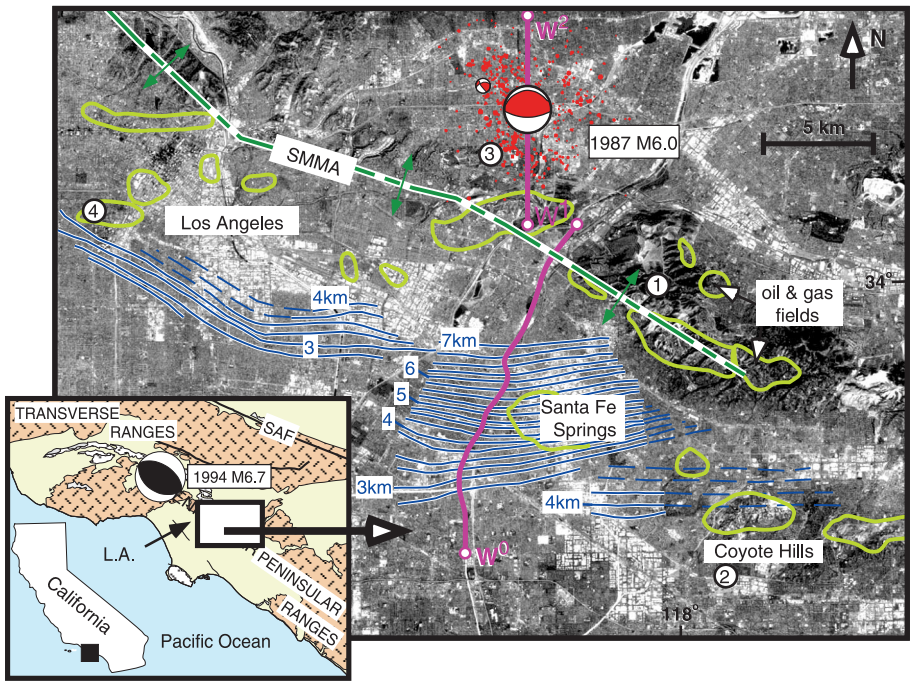

Fig. 2. Contour map of the Puente Hills thrust system with revised locations of the 1987 Whittier Narrows (*M* 6.0) earthquake and aftershocks. The map is overlain on a LandsatTM image (band 5). The inset shows the location of the 1994 Northridge (*M* 6.7) earthquake. SMMA, Santa Monica Mountains anticlinorium (*5*); SAF, San Andreas fault. SCSN seismograph stations: 1, TCC; 2, FLA; 3, GVR; and 4, SC1. Green curves denote locations of oil and gas fields. W^0-W^1 and W^1-W^2 are traces of sections shown in Figs. 1 and 4.

quake position is consistent within the limits of resolution with the projected position of the Puente Hills reflector, offering a compelling linkage between the Santa Fe fault segment and the earthquake (Fig. 4). This linkage implies that the Puente Hills fault system is active and thus warrants consideration as an earthquake hazard.

The Whittier Narrows (M 6) earthquake ruptured only about 10% of the inferred fault area. Assuming that the entire fault system extends to the depth of the Whittier Narrows seismicity, the Los Angeles, Santa Fe Springs, and Coyote Hills fault segments would have areas (*17*) of 280, 260, and 300 km^2, respectively. On the basis of empirical relations between fault rupture area and magnitude (*18*), ruptures on these fault segments could generate 6.5 to 6.6 moment magnitude (M_w) earthquakes. A much larger earthquake (M_w 7.0) could occur if the three fault segments ruptured simultaneously or if the fault system extends below the base of the Whittier Narrows seismicity.

The record of prehistoric ruptures on this system is unknown. Moreover, the number of fault segments and the lack of large events in the historic record (*19*), which dates to about 1850 A.D., make it difficult to forecast future events. Given a range on fault slip rates from 0.5 to 2.0 mm/year (*20–23*) and assuming that this slip is released in M 6.5 to 6.6 earthquakes, each fault segment could rupture every 250 to 1000 years. Multisegment (M_w 7.0) earthquakes would occur less frequently, with a recurrence interval ranging from 500 to 2000 years.

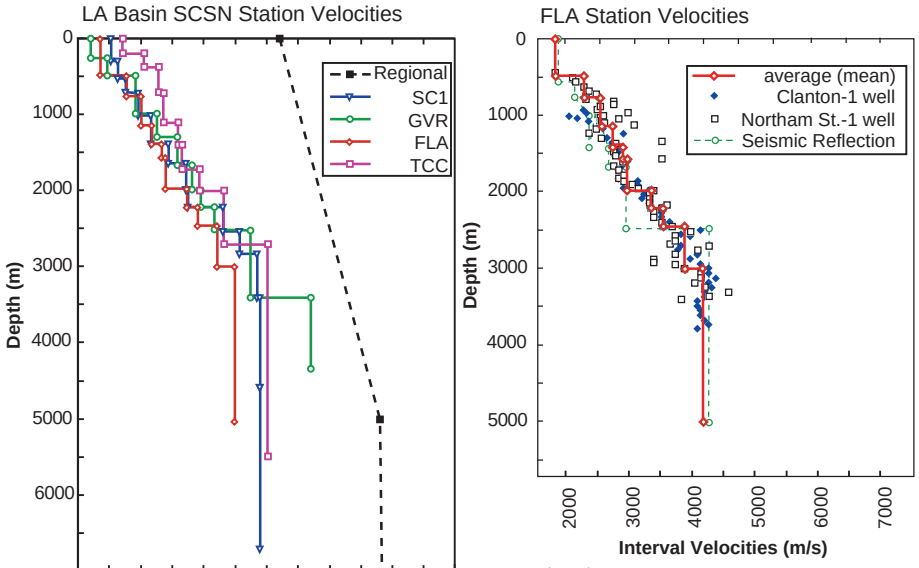

Fig. 3. (Left) Mean velocity functions for four SCSN seismograph stations in the Los Angeles basin derived from industry sonic logs and reflection data. Note the difference between velocity functions and the regional model (*15*) previously used to locate the seismicity. (Right) Sonic log and reflection velocity data used to develop the FLA station function.

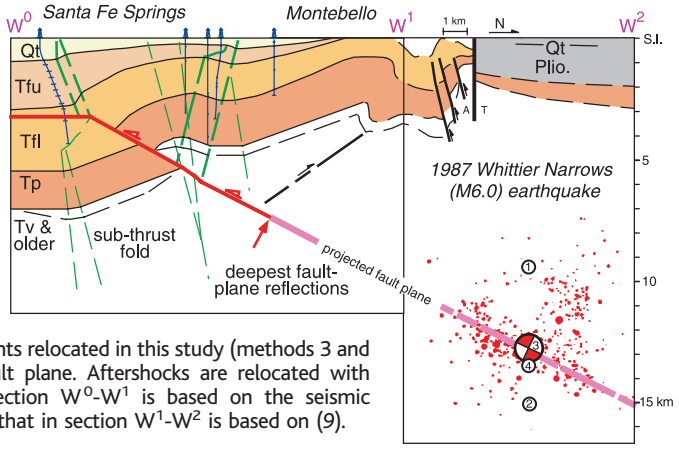

Fig. 4. Geologic cross section of the Santa Fe Springs anticline and fault segment with the relocated mainshock and aftershocks of the 1987 Whittier Narrows earthquake. Mainshock locations: 1, SCSN location; 2, from (*15*); 3, from station terms (*16*); and 4, from SCSN velocity functions (Fig. 3). Note the coincidence of the events relocated in this study (methods 3 and 4) with the projected fault plane. Aftershocks are relocated with method 3. Geology in section W^0-W^1 is based on the seismic reflection image in Fig. 1; that in section W^1-W^2 is based on (*9*).

References and Notes

1. Scientists of the U.S. Geological Survey and the Southern California Earthquake Center, *Science* **266**, 389 (1994).
2. C. M. Rubin, S. C. Lindvall, T. K. Rockwell, *ibid.* **281**, 398 (1998).
3. R. S. Stein and G. Ekstrom, *J. Geophys. Res.* **97**, 4865 (1992).
4. J. Shaw and J. Suppe, *ibid.* **101**, 8623 (1996).
5. T. L. Davis, J. Namson, R. F. Yerkes, *ibid.* **94**, 9644 (1989).
6. J. Suppe, *Am. J. Sci.* **283**, 684 (1983).
7. _____ and D. A. Medwedeff, *Ecologae Geol. Helv.* **83/3**, 409 (1990).
8. R. F. Yerkes, *U.S. Geol. Surv. Prof. Pap. 420-C* (1972).
9. T. L. Wright, in *Active Margin Basins*, K. T. Biddle, Ed., *Am. Assoc. Pet. Geol. Mem.* **52**, 35 (1991).
10. R. S. Yeats and G. J. Huftile, *Southern California Earthquake Center 1996 Annual Report*, (Southern California Earthquake Center, Los Angeles, CA, 1997), vol. II, pp. C75–C79.
11. J. Suppe, G. T. Chou, S. C. Hook, in *Thrust Tectonics*, K. R. McKlay, Ed. (Chapman & Hall, London, 1992), pp. 105–121.
12. The seismic profile presented in Fig. 1 underwent a standard processing routine including normal moveout correction and wave equation migration (Kirchoff F/K domain). The interpreted fault plane is highlighted in red and was selected in a user-defined area by its dip and lateral coherence. Various additional processing steps aimed at reducing noise and eliminating dipping artifacts were applied to the line (not shown), including frequency–wave number (FK) filters and frequency (FX) deconvolution. These steps failed to remove the north-dipping reflections interpreted to represent the fault surface.
13. The Elysian Park fault system forms the overlying Santa Monica Mountains anticlinorium (*5*). Both the fault and the anticlinorium have a northwest-southeast orientation (*4*, *5*) that is distinct from the east-west–striking nodal planes of the 1987 Whittier Narrows mainshock (*14*) and the mapped segments of the Southern Puente Hills blind-thrust system (Fig. 2). Moreover, the Puente Hills fault system lies on top of folds formed above the Elysian Park system (Fig. 1). Thus, we contend that the Elysian Park and Puente Hills fault systems are distinct from one another.
14. E. Hauksson and L. Jones, *J. Geophys. Res.* **94**, 9569 (1989).
15. P. M. Shearer, *ibid.* **102**, 8269 (1997).
16. K. B. Richards-Dinger and P. M. Shearer, *Eos* (Fall Meeting Suppl.) **78**, F445 (1997).
17. Fault areas are taken below 5-km depth, which we consider to be the minimum depth of significant moment release in large earthquakes. Shallower thresholds can be considered with the use of the fault map in Fig. 2.
18. D. L. Wells and K. J. Coppersmith, *Bull. Seismol. Soc. Am.* **84**, 974 (1994).
19. J. F. Dolan *et al.*, *Science* **267**, 199 (1995).
20. Minimum and maximum slip rates are determined on the basis of geologic and geodetic constraints. The geometry of folded growth strata in the Santa Fe Spring structures indicates that at least 800 m of slip occurred on the underlying blind thrust in the Quaternary, with the use of the methods of Suppe *et al.* (*11*) and Shaw and Suppe (*4*). Use of the maximum age of Quaternary strata (1.6. million years ago) yields a minimum slip rate of 0.5 mm/year. Maximum slip rate (2.0 mm/year) is taken as the portion of the shortening (7.5 to 9.5 mm/year) (*21*, *22*) measured by geodesy across the Los Angeles basin that remains unaccounted for on previously recognized fault systems (*23*).
21. Y. Bock *et al.*, *J. Geophys. Res.* **102**, 18013 (1997).
22. Y. Bock and S. Williams, *Eos* **78**, 293 (1997).
23. C. Walls *et al.*, *Nature* **394**, 356 (1998).

24. This research was funded by the Southern California Earthquake Center and data were provided by Texaco. We thank F. Bilotti, K. Bishop, K. Richards-Dinger, J. Dolan, G. Ekström, K. Mueller, and P. Süss for contributions to this work.

24 July 1998; accepted 20 January 1999